Precipitation and Ostwald Ripening in Dilute Al Base-Zr-V Alloys

M. S. ZEDALIS and M. E. FINE

The coarsening rates of both cubic and tetragonal Al_3Zr precipitates in Al were measured. The tetragonal Al_3Zr coarsened 16 times faster than the cubic modification in keeping with the fact that the latter is coherent and coplanar with the matrix while the former forms a semicoherent interface with the matrix giving a larger interfacial energy. Partial substitution of V for Zr reduced the precipitate-matrix mismatch for both phases and slowed both coarsening rates as well as retarded the cubic to tetragonal transformation. Reducing strain and interfacial energy no doubt is the origin of this effect. Since the cubic particles are spherical, their volume fraction is small, and the coherency strains are small, this would appear to be an ideal system for testing the Lifshitz-Slyozov-Wagner theory of diffusion controlled Ostwald ripening. While the theory seems to hold, the calculated diffusivity of Zr in Al is much higher than the value reported in the literature. Because of the low coarsening rates of the dispersed particles, the Al-Zr-V system shows promise as the basis for a high temperature Al alloy.

I. INTRODUCTION

IT seems possible to develop Al-base alloys useful to 375 to 425 °C in view of the behavior of nickel-base alloys which resist degradation of mechanical properties to 75 pct of their absolute melting temperature. For high temperature Al alloys, the dispersed hardening phase must not undergo phase transformation to an undesirable phase during long time exposure at the temperature of interest. Also, if the lattice disregistry across the precipitate/matrix boundary is small, then strong interfaces with low interfacial energy, σ, are expected to exist. In Ostwald ripening, larger particles grow at the expense of smaller ones driven by reduction of the total interfacial free energy. Thus low σ is desirable for the particles to resist coarsening. According to the Lifshitz and Slyozov[1] and Wagner[2] (LSW theory) of diffusion controlled coarsening for dilute dispersions of spherical particles neglecting strain energy, the average precipitate size should increase in accordance to the relationship

$$\bar{r}^3 - \bar{r}_0^3 = k(t - t_0) \qquad [1]$$

where $\bar{r}$ is the average particle radius at time t, $\bar{r}_0$ is the extrapolated value corresponding to t_0, and k represents the rate constant given by

$$k = \frac{8\sigma D C_0 V_m^2}{9\nu RT} \qquad [2]$$

where D is the diffusivity of the rate-controlling solute, C_0 is the solubility limit of that component in the matrix, ν is the stoichiometric factor, and V_m is the molar volume of the dispersed phase. For nondilute solutions, Eqs. [1] and [2] still hold but with another multiplication factor which increases with volume fraction.[3,4] Thus, the ideal dispersed phase should have low interfacial energy, diffusivity, and solubility limit, *i.e.*, low σDC_0, to prevent overaging from bulk diffusion at the temperature of application.

Of course, irrespective of the rate controlling mechanism for Ostwald ripening, a reduction in the total interfacial energy drives the process, and thus a decrease in σ should slow the ripening rate. A number of intermetallic compounds were suggested by one of the authors[5] as candidates for elevated temperature Al alloys based on similarities in structure with aluminum and the possibility of obtaining low values of σ. For the Al_3Zr[6] and Al_3Ti[6,7] tetragonal phases, the lattice mismatches along the a-axis are less than 1 pct and approximately 5 pct, respectively, when compared to Al. It was also suggested[5] that careful selection of alloying elements could further reduce the mismatch, thereby reducing σ.

In a review article, Adam[8] subsequently suggested several Al-base systems containing transition elements for potential elevated temperature use based on low reported values of DC_0 with Zr giving the lowest.

The equilibrium crystal structures of Al_3Zr and Al_3Ti are tetragonal, DO_{23}-type and DO_{22}-type, respectively.[6,7] In dilute Al-Zr alloys an intermediate $L1_2$ structured cubic phase forms initially on aging of supersaturated solid solutions.[9]

While the mismatch between the a lattice parameters of Al and tetragonal Al_3Zr is slightly less than 1 pct, the c lattice parameter of Al_3Zr is approximately 4 times a(Al), the actual ratio $c(Al_3Zr)/a(Al)$ being 4.28. It was reasoned that a lower interfacial energy might result if this ratio were nearer to 4. Substitution of V for Zr[10,11] was found to have little effect on the mismatch in the a direction but the ratio $c[Al_3(V_{0.875}Zr_{0.125})]/a(Al)$ was reduced to 4.20. This gave an average total mismatch, δ, defined as

$$\delta = \frac{2[a(Al) - a(Al_3X)]}{3a(Al)} + \frac{[c(Al_3X) - 4a(Al)]}{12a(Al)} \qquad [3]$$

of 0.0239 compared to 0.0288 for Al_3Zr. Increasing the V beyond 0.875 resulted in transformation to the DO_{22} structure and poorer overall mismatch.

The objective of the present study was to compare the Ostwald ripening kinetics of the metastable cubic ($L1_2$) and the equilibrium tetragonal (DO_{23}) Al_3Zr and $Al_3(V_{0.875}Zr_{0.125})$ precipitates in dilute Al alloys. Decomposition from the supersaturated solid solutions and the $L1_2 \rightarrow DO_{23}$ transformation were also studied. Because of the low rates of Ostwald ripening, both $L1_2$ and DO_{23} structured Al_3(V, Zr) dispersed phases show promise for use in elevated temperature Al alloys.

M. S. ZEDALIS is Research Metallurgist with Allied Chemical Corporation, Morristown, NJ 07960. M. E. FINE is Professor, Department of Materials Science and Engineering, Northwestern University, Evanston, IL 60201.

Manuscript submitted February 10, 1986.

II. EXPERIMENTAL PROCEDURES

Alloys of the compositions shown in Table I were prepared by arc melting 5-gram samples in a gettered argon atmosphere using a tungsten electrode and a water-cooled copper cathode crucible. The cooling rate was rapid enough so that dilute supersaturated solid solutions were produced; *i.e.*, the melting and rapid freezing and cooling served as the solution treatment. The Al was 99.996 pct pure, the V was Johnson-Mathey spectrochemical grade, and the Zr was cut from a crystal bar prepared by thermal reduction of iodides. The alloy concentrations were selected[12,13] to give approximately 1 vol pct of tetragonal precipitate at the aging temperature of 375 °C.

To suppress a cellular mode of precipitation, cold working prior to aging or preaging for a short time (0.5 or 1 hour) at 500 °C was done. Tetragonal (DO_{23}) Al_3Zr precipitate samples were obtained by 95 pct cold rolling and annealing at 600 °C for 50 hours. For the Al-V-Zr alloy (1VZ) an additional 5 pct cold rolling and annealing for 50 hours at 600 °C were necessary to transform completely the precipitates to the tetragonal (DO_{23}) structure. Aging was carried out in a vacuum of better than 5×10^{-6} torr with the temperature being controlled to ±1 °C. All specimens were air cooled following aging.

Foils for TEM examination (Hitachi H-700H at 175 kV) were prepared by electropolishing in a solution of 80 pct CH_3OH-20 pct HNO_3 at 95 mA and −70 °C. Electron diffraction was used to measure the lattice parameter of the metastable ($L1_2$) phase by applying the techniques outlined by Hirsch *et al.*[14] and Edington.[15] The volume fraction and particle sizes were too small to conveniently use X-rays. The expected accuracy by this method is less than 0.5 pct. The precision is better than the accuracy.

Particle size measurements were made from dark-field electron micrographs obtained by using superlattice reflections with the particle diameter being taken as the line of no contrast. To obtain average particle sizes, approximately 400 to 800 particles were measured. The particle size distribution functions, $\rho^2 h(\rho)$, were empirically calculated according to[17]

$$\rho^2 h(\rho) = \frac{N(r, r + r)}{\Sigma N(r, r + r)} \frac{\bar{r}}{\Delta r} \frac{9}{4}. \qquad [4]$$

To estimate the Zr concentration in the Al solid solution and its effect on the lattice parameter of the Al solid solution at 425 °C, X-ray diffraction was performed at temperature on −150 mesh (~100 μm) powder samples of the Al solid solution containing either the metastable, cubic ($L1_2$) Al_3Zr phase or the equilibrium, tetragonal (DO_{23}) Al_3Zr phase. Only the lattice parameter of the solid solution was measured. To remove any residual stresses incurred during filing, specimens were annealed at 330 °C for 4 hours. Diffraction data were obtained with CuKα radiation in a Norelco X-ray diffractometer with an attached heating stage. Temperatures were maintained at 425 ± 10 °C while data were being acquired. Only peak positions corresponding to the higher order planes were analyzed using a 10-second count time in the step scan mode at increments of 0.02 deg. Specimen alignment errors were determined by the lattice parameter calculated for a Si standard mixed with the alloy powder.

Table I. Compositions of Alloys

Alloy	Nominal Weight Percent Zr	Nominal Weight Percent V	Analyzed Weight Percent Zr	Analyzed Weight Percent V
1Z	0.75	—	0.79	0.00
1VZ	0.10	0.40	0.10	0.35
2VZ	0.23	0.34	—	—

III. RESULTS AND DISCUSSION

A. *Matrix Solute Concentration in Alloy Containing Metastable, Cubic ($L1_2$) Al_3Zr Precipitates*

In the Al-Zr system, when there is equilibrium between the tetragonal (DO_{23}) phase and the matrix, C_0 may be obtained directly from the equilibrium phase diagram. However, when the metastable, cubic ($L1_2$) Al_3Zr phase is present, thermodynamics predicts that the metastable equilibrium solubility limit in the Al solid solution matrix is greater than that given by the equilibrium phase diagram.

The dissolved Zr concentration in the Al matrix in metastable equilibrium with cubic Al_3Zr at 425 °C was estimated by X-ray diffraction analyses as shown in Figure 1. The open circle corresponds to the lattice parameter of pure Al at 425 °C after correcting for thermal expansion.[18] The closed circle represents the lattice parameter measured for the Al(ss) in equilibrium with the tetragonal Al_3Zr phase at 425 ± 10 °C. Thus, based on the lattice parameter measured for the Al(ss) in the presence of the cubic Al_3Zr phase at 425 ± 10 °C, a Vegard's law extrapolation predicts that the Zr concentration in solution at 425 °C is 0.0426 at. pct Zr. An appropriate solvus line for the Al solid solution in equilibrium with cubic Al_3Zr may then be drawn predicting for 375 and 400 °C, C_0 values of 0.0380 and 0.0395 at. pct, respectively.

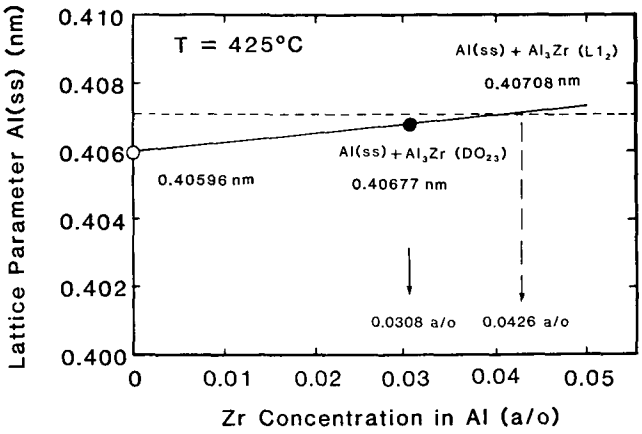

Fig. 1 — Variation of lattice parameter of Al solid solution with Zr content. The horizontal dashed line is the lattice parameter for the Al(ss) in metastable equilibrium with cubic Al_3Zr which predicts by extrapolation a solubility limit of 0.0426 at. pct Zr in Al at 425 °C.

B. *Lattice Disregistry between the Al(ss) and Cubic ($L1_2$) Al_3Zr and $Al_3(Zr,V)$*

For measuring the lattice parameter mismatch between the Al(ss) and the cubic $Al_3(Zr, V)$ precipitates with varying Zr/V ratio, selected area electron diffraction (SAD) patterns were obtained from areas in the matrix containing a relatively high density of particles. The results of the electron diffraction analyses of specimens containing Al_3Zr, $Al_3(V_{0.725}Zr_{0.275})$ and $Al_3(V_{0.875}Zr_{0.125})$ precipitates, isothermally aged at 425 °C for various lengths of time, are shown in Figure 2. The horizontal dashed line represents the lattice parameter of Al. Values of δ were determined directly from the differences in spacing of the $L1_2$ and matrix spots for long aging times. As shown in Figure 2, the improved lattice matching previously reported for the equilibrium, tetragonal $Al_3(V_{0.875}Zr_{0.125})$ phase with the Al matrix over the unalloyed Al_3Zr[11] is also found with the metastable, cubic ($L1_2$) phases.

The value of the $L1_2$ Al_3Zr lattice parameter appears to increase with aging time. This affect was carefully checked to make sure it is not spurious. A similar result for β' NiAl precipitates in Fe-Ni-Al alloys was obtained by H. Calderon (private communication). This effect is not seen with the Al-V-Zr samples where the mismatch is smaller. It might be due to a change in composition of the precipitate with aging or to imperfections or concentration changes at or near the interface to reduce coherency strain energy.

Assuming Vegard's law, the lattice parameter variation of cubic $Al_3(V_xZr_{1-x})$ at various concentrations of x is predicted in Figure 3. The lattice parameters of cubic ($L1_2$) Al_3X-type intermetallic phases were estimated from the atomic sizes[19] of the elements Li, Hf, Nb, Ta, Ti, V, Zr, Y, assuming close packing of hard spheres of the ordered fcc unit cell. The calculated lattice parameter for the cubic Al_3Zr phase is somewhat larger than that measured by electron diffraction (0.431 nm *vs* 0.410 nm). Of all the compounds calculated, only Al_3V (0.393 nm) has a smaller lattice parameter than Al. Thus V addition to Al_3Zr is predicted to reduce the mismatch with the matrix as already shown to occur in Figure 3. Vanadium as an alloying element was selected on this basis.

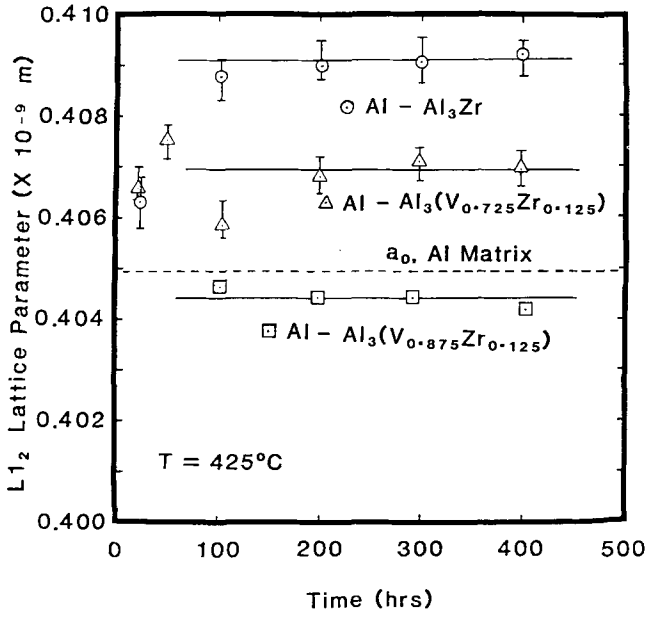

Fig. 2—Aging time dependence of the lattice parameters of cubic ($L1_2$-structure) Al_3Zr, Al-$Al_3(V_{0.725}Zr_{0.125})$, and $Al_3(V_{0.875}Zr_{0.125})$. The aging temperature was 425 °C, but the lattice parameter measurements were made at room temperature.

C. *Isothermal Aging of Al-Zr and Al-V-Zr Solid Solutions at 375 °C*

The precipitation studies were initially done by isothermally aging supersaturated solid solutions of alloys 1Z and 2ZV at 375 °C. Neither electron nor light microscopy revealed the presence of any second phase particles in the as-cast microstructure. Decomposition from the supersaturated solid solution was observed in both alloys to occur by a cellular discontinuous mode of precipitation, the product being cubic $L1_2$ structured Al_3X and the depleted solid solution. This agrees with previous studies performed on the Al-Zr[20,21,22] and Al-Hf[23,24] systems. Migrating grain boundaries act as natural sinks for solute atoms and leave cellular precipitates behind in their wakes. Even following 300 hours of aging at 375 °C, selected area electron diffraction revealed that the precipitates remained cubic ($L1_2$) in structure with no evidence of the DO_{23} structure.

D. *Decomposition of the Al-Zr and Al-V-Zr Solid Solutions on Aging at 450 °C after 95 Pct Cold Rolling*

To eliminate discontinuous precipitation and accelerate the precipitation process, a second set of samples was cold rolled 95 pct prior to isothermal aging at 450 °C. Cold rolling was found to enhance the kinetics of decomposition of the dilute Al-Zr solid solution from that previously reported[9,21–24] for aging at 450 °C. This also occurred for the Al-V-Zr supersaturated solid solution. Again, neither optical nor electron microscopy revealed the presence of any particles in the as-cast and rolled samples. In the Al-Zr alloy following 0.5 hour of aging at 450 °C, spherical, approximately 15 nm $L1_2$ particles appeared in a rather inhomogeneous distribution throughout the matrix. They were typically associated with dislocations and subgrain boundaries. Following 5 hours

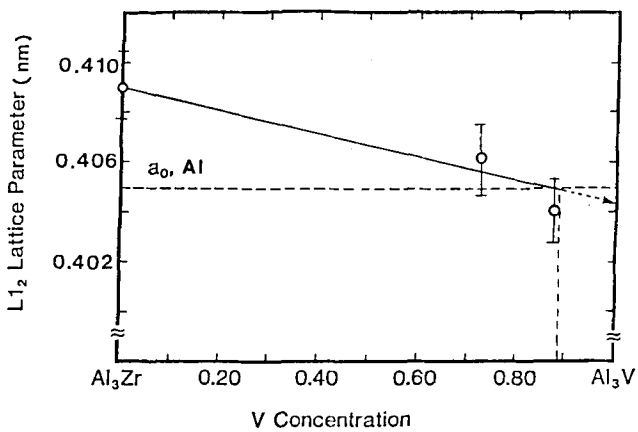

Fig. 3—Lattice parameter of cubic $L1_2$ $Al_3(Zr, V)$ *vs* vanadium concentration expressed as the V/Zr atom fraction ratio.

aging, spherical Al_3Zr particles were often seen connected by dislocations (Figure 4). Such connecting dislocations may act as conduits for solute diffusion and may assist in the coalescence of spherical precipitates and formation of rod-shaped precipitates such as seen in Figure 4. Numerous models have been proposed to explain the formation of these rods; however, weak-beam–dark-field micrographs, Figure 4, support the model proposed by Nes.[9] Here, precipitation on a dislocation associated with helical climb appears to be responsible for the formation of these rod-shaped precipitates. Furthermore, the associated interfacial dislocation network and the absence of matrix strain contrast are indicative of a precipitate which is semi-coherent.

The present results thus support both models proposed independently, for the formation of rod-shaped $L1_2$ precipitates (not the "fan-shaped" cellular decomposition product). Izumi and Oelschlagel[21,22] proposed that the formation of rod-shaped precipitates are a result of coalescence of particles. Some rod-shaped precipitates shown in Figure 4 appear to be the direct result of coalescence. As predicted by the Gibbs-Thomson-Fruendlich equation, the small radii of curvature at the neck of coalesced precipitates will rapidly increase, eventually resulting in the formation of a well-defined rod-shaped precipitate particle. As already mentioned, precipitation on a dislocation associated with helical climb is seen in Figure 4. Through the generation of vacancies, such helical dislocations wrapped around the precipitate may promote a preferential growth direction as well as enhance the growth kinetics by sweeping up nearby solute atoms with their wandering tails with subsequent rapid pipe diffusion.

The first appearance of the equilibrium, tetragonal Al_3Zr phase was after 15 hours of aging at 450 °C. After 20 hours of aging, the DO_{23} precipitates were platelike with faceted caps (Figure 4), and in some cases demonstrated an orientation within the Al matrix identical to that found by Izumi and Oelschlagel,[21] *i.e.*,

$$\langle 001 \rangle_{Al_3Zr} \| \langle 001 \rangle_{Al} \qquad (100)_{Al_3Zr} \| (100)_{Al}$$

Following 50 hours of aging (data not shown), the major axes of some of the tetragonal particles were observed to lie also along [111] directions.

An identical study was performed on the Al-V-Zr alloy containing $Al_3(V_{0.875}Zr_{0.125})$. Though the overall sequence of decomposition was identical to that observed for the unalloyed Al_3Zr phase, the kinetics were appreciably more

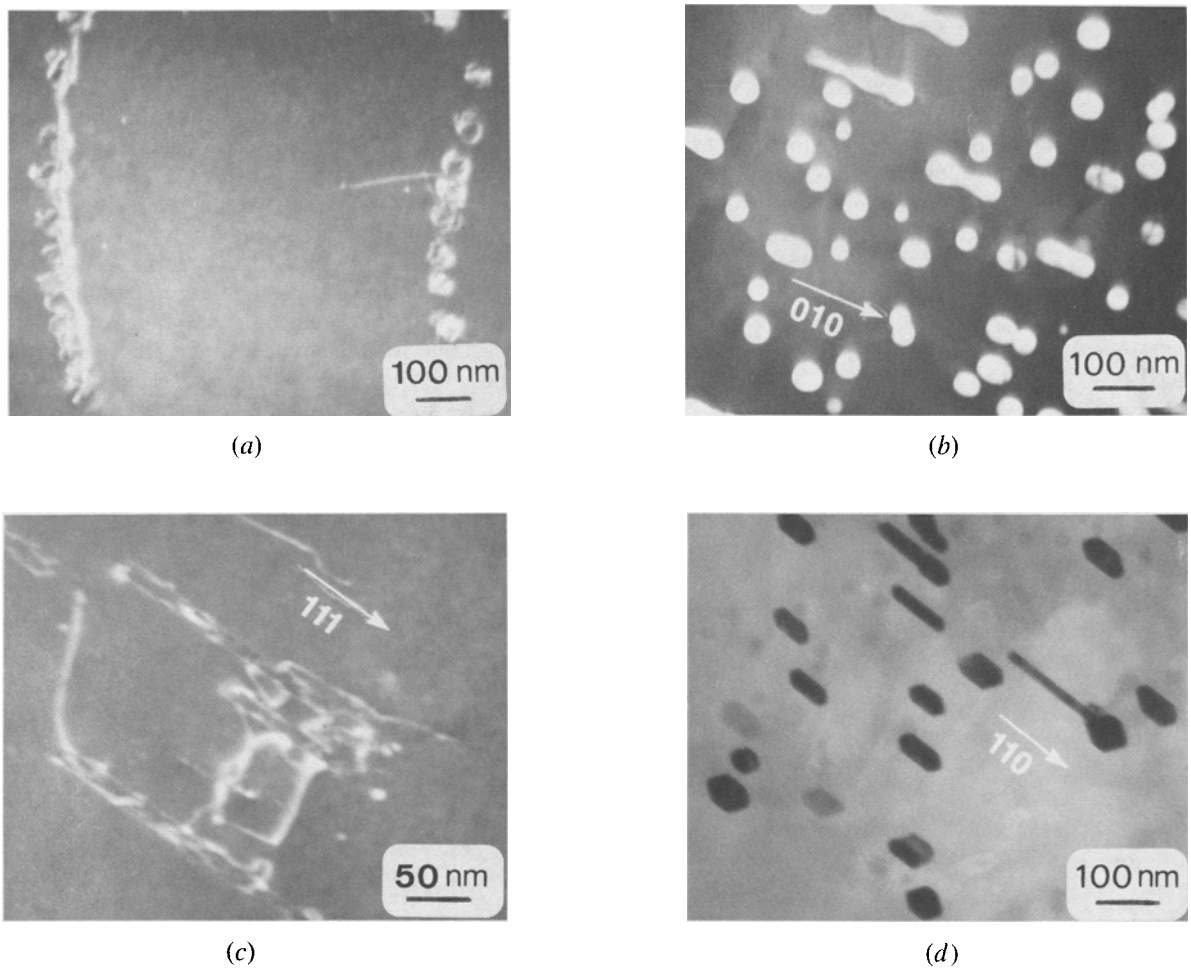

Fig. 4—TEM micrographs showing stages of precipitation of Al_3Zr at 450 °C following 95 pct cold rolling. (*a*) shows cubic $L1_2$ precipitates on dislocations after 5 h aging, (*b*) shows an area where general precipitation of the cubic phase occurred after 10 h of aging, (*c*) is a weak-beam–dark-field TEM showing precipitation of the cubic phase on dislocations after 13.5 h of aging, and (*d*) shows tetragonal DO_{23} Al_3Zr precipitates after 20 h of aging.

sluggish. For the cubic $Al_3(V_{0.875}Zr_{0.125})$ phase, coalescence and the formation of rod-shaped precipitates was not observed until after 20 hours of aging at 450 °C (Figure 5). This is in comparison to 13.5 hours of aging for the binary Al-Zr alloy. The tetragonal phase was not observed until after 100 hours of aging (Figure 5) compared to 15 hours for the binary alloy.

The present results thus show that reducing the lattice disregistry decreases the decomposition kinetics (or increases the stability) of cubic $L1_2$ particles. The cubic Al_3Zr and $Al_3(V_{0.875}Zr_{0.125})$ precipitates have mismatches of approximately 1.0 ± 0.2 pct and -0.1 ± 0.2 pct, respectively. The increased stability of the metastable cubic ($L1_2$) $Al_3(V_{0.875}Zr_{0.125})$ precipitates *vs* the cubic Al_3Zr precipitates is attributable to reduced matrix/precipitate strain energy and/or lower interfacial energy. For the cubic Al_3Zr particles, the average particle radius approaches 16 nm prior to the initial observance of the tetragonal phase; however, this average radius is approximately 20 nm for the $Al_3(V_{0.875}Zr_{0.125})$ particles. As subsequently described, since the growth rate of the latter is slower, this corresponds to a much longer transformation initiation time.

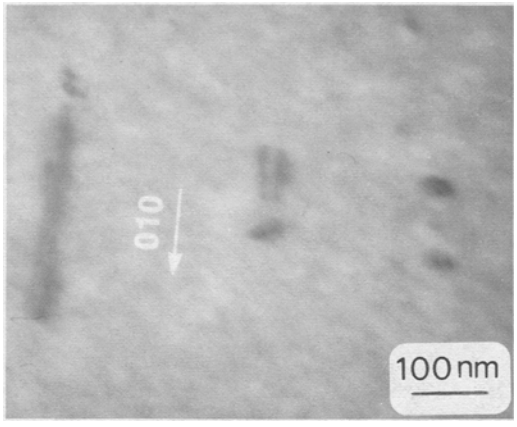

(*a*)

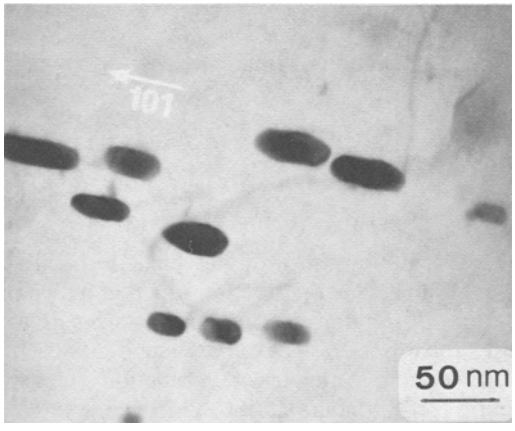

(*b*)

Fig. 5—TEM micrographs showing stages of precipitation of $Al_3(V_{0.875}Zr_{0.125})$ at 450 °C: (*a*) after 20 h of aging, rod-shaped as well as spherical cubic $L1_2$ precipitates are seen; (*b*) after 100 h of aging, tetragonal DO_{23} precipitates are seen.

E. *Decomposition of the Al-Zr Solid Solution: 95 Pct Cold Rolled and Aged at 600 °C*

With Al-Zr specimens initially cold rolled 95 pct and isothermally aged at 600 °C, copious precipitation was observed almost immediately in the form of small, approximately 10 nm spherical $L1_2$ type particles. Following 12 hours of aging at 600 °C, some of the particles were observed to be lenticular in shape and oriented along [110] directions (Figure 6). It is apparent that these lenticular particles are growing at a faster rate than the smaller spherical particles. Weak beam-dark field imaging revealed a strong interaction between such particles and glissile dislocations. Sharp lines of no-contrast are observed in some of the precipitates and thought to be antiphase domain boundaries (APB) (Figures 6(a) and (c)). The authors were not able to identify the crystal structure of these lenticular precipitates; however, the appearance of such a sharp line of no contrast is similar to the APB's observed in $AuCu_3$ specimens[25] supporting Ryum's model for the transformation from the cubic ($L1_2$) phase to an imperfect tetragonal (DO_{23}) phase by the formation of an APB with a displacement vector $\mathbf{R} = a/2$ [110] on [100] type planes.[26]

An imperfect DO_{23}-type crystal structure may be formed from an $L1_2$-type structure by an atomic displacement of $a/2$ [110] on particular (001) planes of the $L1_2$ lattice.[27] Based on the analysis by Weatherly[28] of the formation of APB's in Al-Cu alloys, it was concluded that precipitate coalescence and precipitate/dislocation interaction are two modes of forming an antiphase domain boundary in a precipitate. An APB may be formed if glissile dislocations in the matrix have sufficient enough energy to cut through the precipitate. Since a transformation occurs which lowers the free energy, then negative energy is required for this cutting. Weak beam-dark field imaging (Figure 6(b)) appears to show a dislocation actually cutting a large lenticular $L1_2$ particle.

With continued aging (Figure 6(d)), all of the particles were observed to become lenticular in shape prior to forming the equilibrium tetragonal structure, as verified by electron diffraction.

F. *Coarsening Kinetics of Cubic ($L1_2$) Al_3Zr and $Al_3(V, Zr)$ Precipitates*

The coarsening kinetics of the binary cubic ($L1_2$) Al_3Zr precipitates isothermally aged at 375 °C, 400 °C, and 425 °C are shown in Figure 7. Particles associated with dislocations were not included in the analyses. The particle sizes for short aging times are, of course, dependent on the prior treatment. As observed by others,[22] the density of precipitates is not uniform in the samples but varies somewhat from place to place. The sampling of particles is tilted toward the higher density regions since more particles were found in these regions. Extensive cold work had the effect of giving a more uniform particle distribution after aging, but in this series of experiments the samples were not cold worked. As predicted by the LSW theory of VDC coarsening, a linear relationship between the cube of the average particle radius and time is more or less obtained at all temperatures investigated. Through a least squares analysis, the coarsening rates k in Eq. [1] and the coefficient of linearity were calculated and are reported in Table II. Typical micrographs are shown in Figure 8.

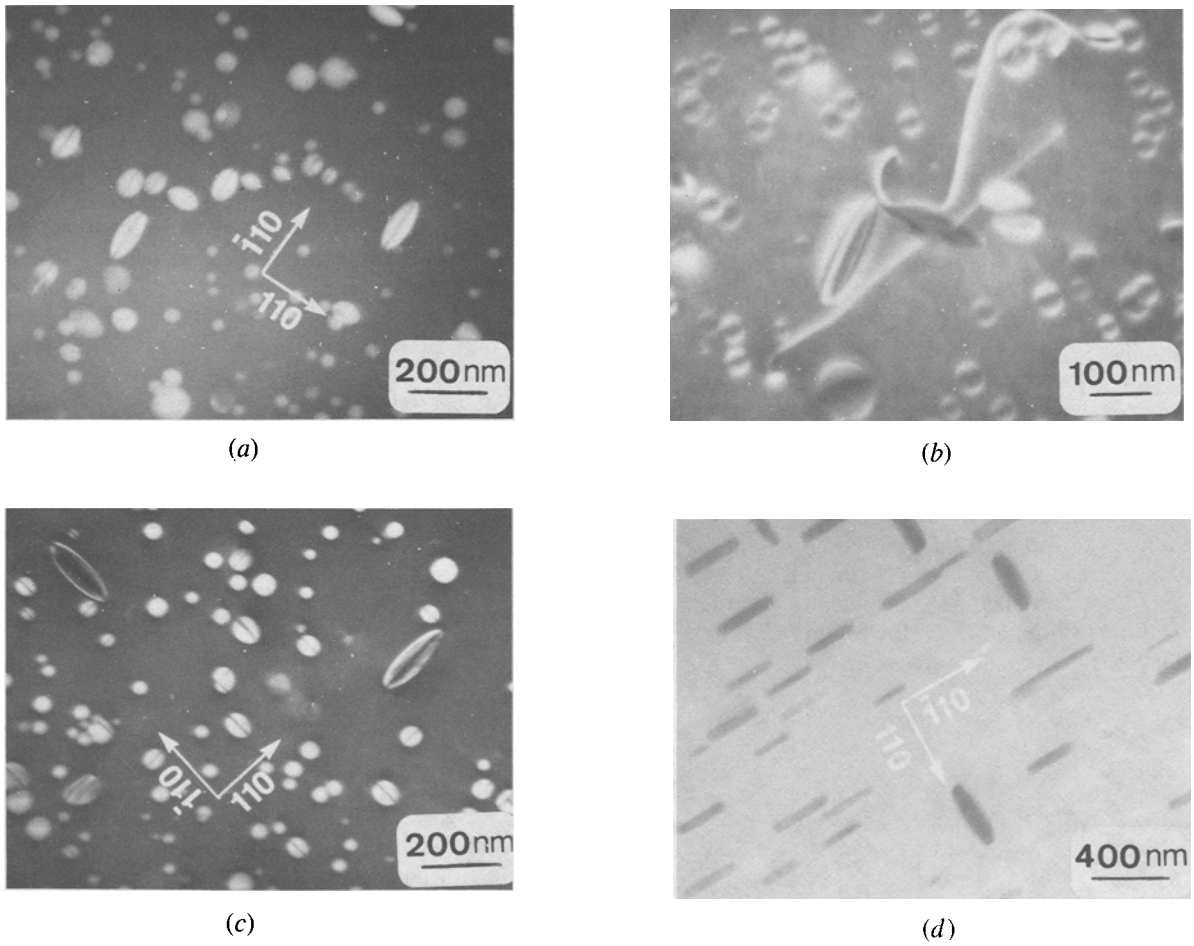

Fig. 6—TEM micrographs documenting transformation of cubic $L1_2$ Al_3Zr to an imperfect tetragonal "DO_{23}" Al_3Zr structure during aging at 600 °C after 95 pct cold rolling. Explanations are in text. (*a*) and (*b*) are after 12 h, (*c*) is after 15 h, and (*d*) is after 25 h of aging.

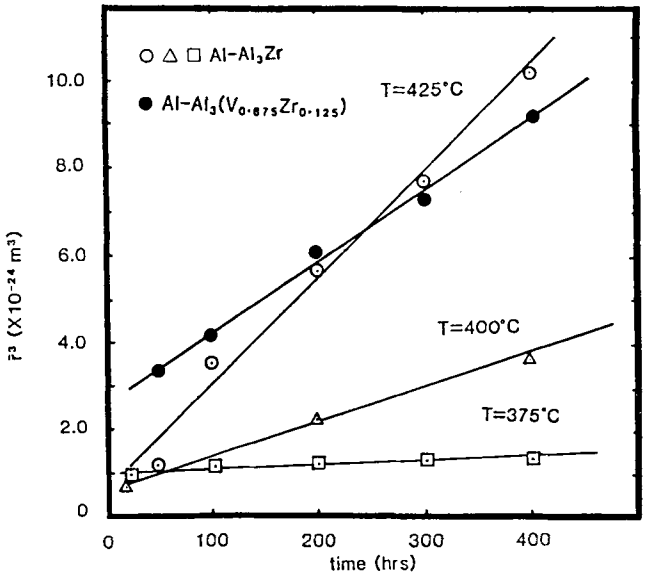

Fig. 7—Coarsening kinetics of cubic $L1_2$ Al_3Zr precipitates during isothermal aging at 375, 400, and 425 °C. $\bar{r}$ is the average particle radius at a particular time t. Specimens aged at 375 °C and 400 °C were preaged at 500 °C to eliminate cellular precipitation. It was not necessary to preage the specimens aged at 425 °C since cellular precipitation was not observed at this aging temperature. Coarsening kinetics of Al-$Al_3(V_{0.875}Zr_{0.125})$ at 425 °C is also shown.

Some particle size distributions (PSD) for the cubic Al_3Zr precipitates at each temperature investigated are given in Figure 9. At least 500 particles were measured for each distribution curve. The solid line in each figure represents the "quasi-steady-state" distribution predicted by the LSW theory of Ostwald ripening and given by the function

$$f(r,t) = g(t)\rho^2 h(\rho) \qquad [5]$$

where $g(t)$ is a function of time only, $\rho = r/\bar{r}$, and $h(\rho)$ is given by

$$h(\rho) = [3/(\rho + 3)]^{7/3}[(-3/2)/(\rho - 3/2)]^{11/3} \cdot \exp[\rho/(\rho - 3/2)] \qquad [6]$$

when $\rho < 3/2$; $h(\rho) = 0$ when $\rho \geq 3/2$.

Of the distributions shown, only that for 200 hours at 375 °C obeys the LSW distribution function which predicts a rapid drop-off in number of particles at sizes greater than the most probable size. The others (such as 400 hours at 425 °C) have more symmetrical distributions; however, the distribution for 400 hours at 400 °C is askew in the opposite sense.

The coarsening kinetics of the cubic ($L1_2$) $Al_3(V_{0.875}Zr_{0.125})$ phase isothermally aged at 425 °C is also shown in Figure 7. Table II also gives the calculated coarsening rate constants and values of the coefficient of linearity. Some measured particle size distributions are given in Figure 10.

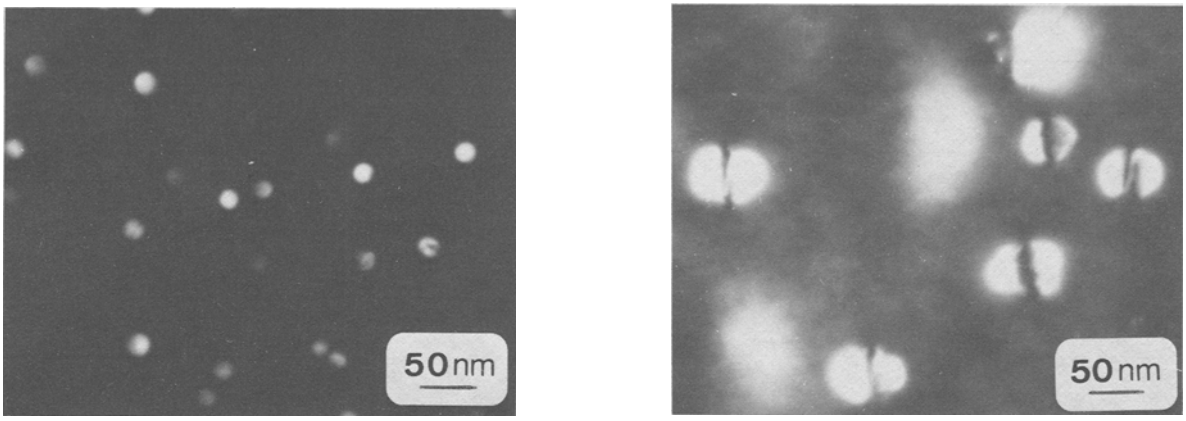

(*a*) (*b*)

Fig. 8—TEM micrographs documenting coarsening of cubic $L1_2$ Al_3Zr after 20 and 200 h of aging at 425 °C.

In keeping with the lower mismatch, the coarsening rate for the cubic $Al_3(V_{0.875}Zr_{0.125})$ precipitates is slower than for Al_3Zr. Again, the distributions shown do not obey the LSW distribution function even though there is a reasonable fit of the $\bar{r}^3$ *vs t* data to a straight line.

In an effort to reach a later stage of aging to see if the LSW size distribution was achieved, a sample with $Al_3(V_{0.725}Zr_{0.275})$ particles was preaged for 1 hour at 500 °C prior to aging at 425 °C. As shown in Figure 11, there does seem to be good agreement with predictions of the LSW theory. Also, the rate constant determined from a straight line drawn through the $\bar{r}^3$ *vs t* data plot was 2.26×10^{-26} m^3/hr with a coefficient of linearity of 0.99 which is intermediate between that for cubic Al_3Zr and Al_3

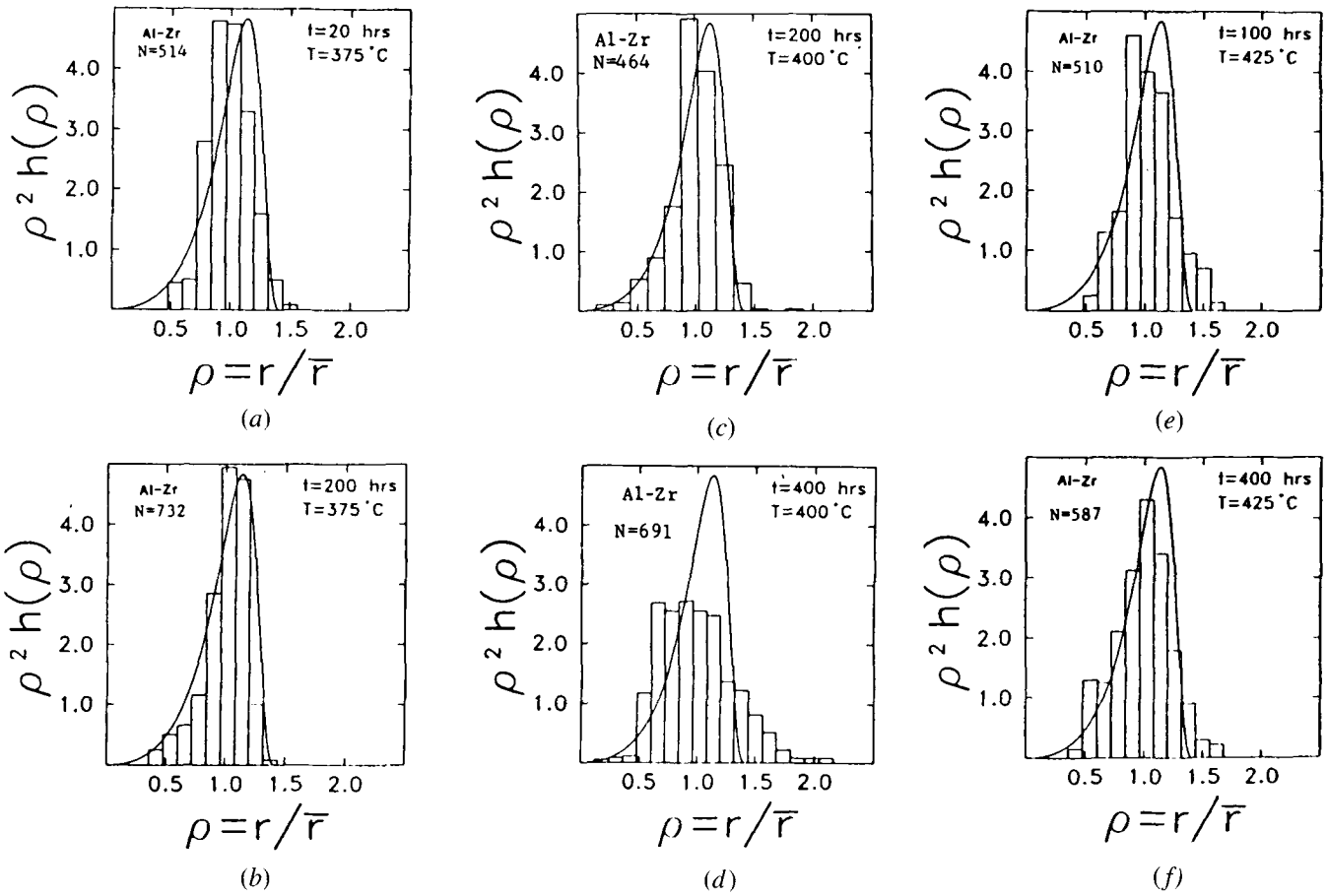

Fig. 9—Normalized particle size distributions for cubic Al_3Zr aged for various times at 375, 400, and 425 °C. The solid curve shows the predicted LSW distribution. For the 375 and 400 °C aging, the specimens were preaged 0.5 h at 500 °C. (*a*) 20 h at 375 °C, (*b*) 200 h at 375 °C, (*c*) 200 h at 400 °C, (*d*) 400 h at 400 °C, (*e*) 100 h at 425 °C, and (*f*) 400 h at 425 °C.

Table II. Measured Coarsening Rate Constants and Coefficients of Linearity for the Cubic ($L1_2$) Particles Aged at 375 °C, 400 °C, and 425 °C

Cubic Phase	Temperature (°C)	Mismatch (δ)	Measured Volume Coarsening Rate Constant (m^3/hr)	Coefficient of Linearity
Al_3Zr	375*	1.0	1.22×10^{-27}	0.92
Al_3Zr	400*	1.0	7.50×10^{-27}	0.99
Al_3Zr	425	1.0	2.49×10^{-26}	0.97
$Al_3(V_{0.875}Zr_{0.125})$	425	−0.1	1.63×10^{-26}	0.99
$Al_3(V_{0.725}Zr_{0.275})$	425**	0.46	2.26×10^{-26}	0.99

*Preaged for 0.5 hour at 500 °C prior to isothermal aging.
**Preaged for 1 hour at 500 °C prior to isothermal aging.

($V_{0.875}Zr_{0.125}$) in keeping with the intermediate value of mismatch.

G. *Temperature Dependence of Ostwald Ripening*

The coarsening rate constant, k, in the LSW theory of VDC coarsening is given by the expanded expression

$$k = \frac{8\sigma C_0 V_m^2 D_0 \exp(-Q/RT)}{9\nu RT} . \quad [7]$$

Rearranging terms and taking logarithms gives the linear equation

$$\ln(KT/C_0) = \ln A - (Q/RT) \quad [8]$$

where $\ln A$ is the y-intercept given by

$$\ln A = \ln(8/9)(\sigma D_0 V_m^2)/(\nu R) . \quad [9]$$

Thus, from a plot of $\ln(KT/C_0)$ *vs* $1/T$, assuming A is constant, it is possible to determine empirically the activation energy, Q, for Zr diffusion in the Al matrix if the diffusion of Zr is indeed controlling coarsening. The value of the activation energy for Al diffusion in the Ni-base systems determined in this manner by Ardell and Nicholson[17] was found to be in excellent agreement with the value of activation energy determined by conventional methods.

By the radiotracer technique,[28] values for D_0 and Q of 7.28×10^4 mm^2/sec and 242 kJ/mole, respectively, were

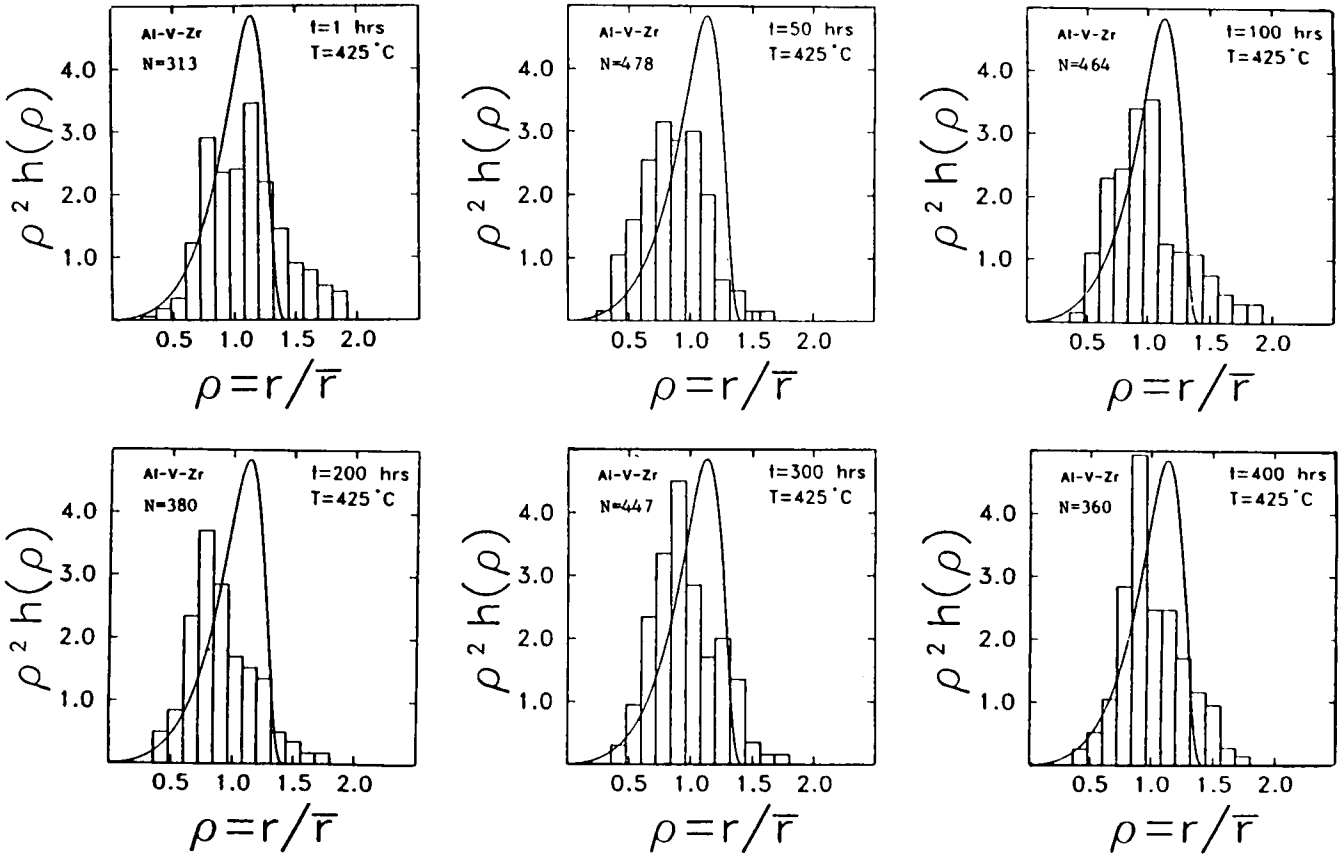

Fig. 10—Normalized particle size distributions for cubic $Al_3(V_{0.875}Zr_{0.125})$ aged from 1 to 400 h at 425 °C. The solid curve shows the predicted LSW distribution.

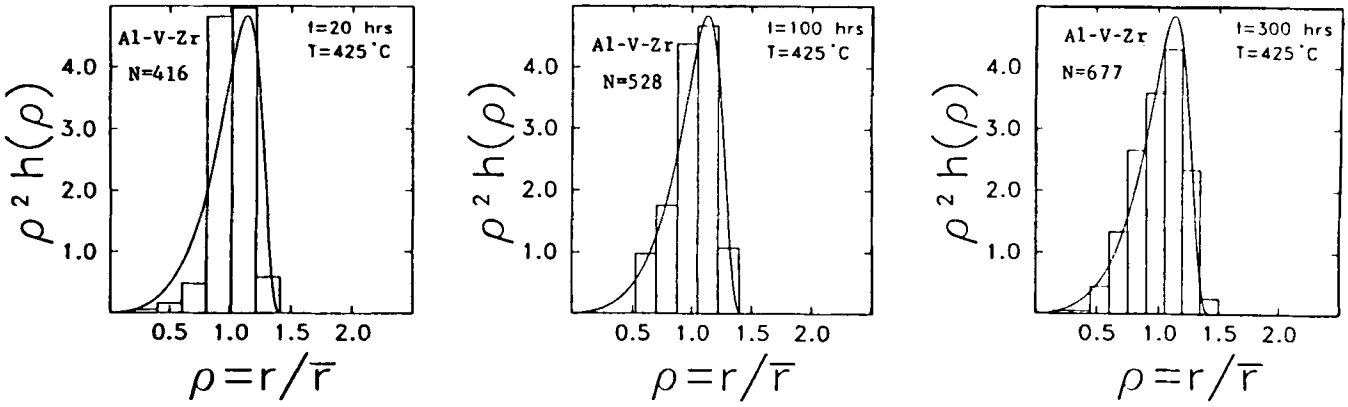

Fig. 11 — Normalized particle size distributions for cubic $Al_3(V_{0.725}Zr_{0.275})$ aged for 20, 100, and 300 h at 425 °C. In order to try to achieve a steady distribution, the specimens were preaged for 1 h at 500 °C. The solid curve shows the predicted LSW particle size distribution. Note the agreement between measurements and theory is much better than in Fig. 10 where the samples were not preaged.

determined for the diffusivity of Zr in Al. However, recent measurements[29] of the decomposition of supersaturated Al-Zr solid solutions indicate that diffusion of Zr in Al occurs at a much faster rate than predicted. Jones[29] suggested values of D_0 and Q of approximately 30 mm^2/sec and 186 kJ/mole, respectively. Recently, Hori *et al.*[30] investigated the early growth rates of Al_3Zr precipitates in Al-0.22 wt pct Zr alloys and proposed an activation energy of approximately 217 kJ/mole.

A plot of $\ln(KT/C_0)$ *vs* $1/T$, corresponding to the coarsening rates measured for the cubic ($L1_2$) Al_3Zr particles at 375 °C, 400 °C, and 425 °C is shown in Figure 12. From a least squares analysis, an effective activation energy for Zr diffusion in the Al matrix was calculated to be 222 kJ/mole. This is close to the value determined by Hori *et al.*

H. *Calculation of the Effective Interfacial Energies*

Since the Al-Zr alloy studied is dilute and the particles are spherical, an accurate calculation of the interfacial energy between Al_3Zr and the Al from the LSW equation for VDC was anticipated. Assuming the radiotracer measured D at 640 °C is accurate but assuming the correct value of Q is 222 kJ/mole, a D_0 of 5400 mm^2/sec is computed. This gives D_{Zr} at 425 °C of 1.4×10^{-19} m^2/sec. With C_0 of 43 moles Zr/m^3 and V_m of 4.13×10^{-5} m^3/mole and taking Wagner's stoichiometric factor $\nu = 1$, an interfacial energy of 4 J/m^2 is calculated. This is a hundred times larger or more than expected for the interfacial energy between the coherent cubic Al_3Zr and the Al matrix. If the radiotracer Q is used to determine D at 425 °C, the agreement is even worse. Similar studies on Ni-base alloys[17,31,32] and Fe-Ni-Al alloys[33,34] where similar coherent precipitates form have yielded σ values of 0.01 to 0.03 J/m^2. We are not able to explain this discrepancy at this time. Ostwald ripening occurs much more rapidly than predicted by the LSW theory. The nonuniform distribution of precipitates may be playing a role. As already mentioned, 95 pct cold rolling prior to aging at 450 °C gave a much more uniform precipitate distribution. The cold rolling also increased the rate constant by a factor of 2. Although particles at grain boundaries or on dislocations were not included in the particle size measurements, imperfections may be playing a role to increase the coarsening rate.

Reducing the mismatch and thus σ by adding V does, however, reduce the coarsening rate in keeping with the predictions of the LSW theory but, of course, since Ostwald ripening is driven by reduction in total surface energy, any theory for Ostwald ripening must make the same prediction.

I. *Coarsening Kinetics of Tetragonal Al_3Zr and $Al_3(V_{0.875}Zr_{0.125})$ Precipitates*

The coarsening kinetics of the tetragonal (DO_{23}) Al_3Zr and $Al_3(V_{0.875}Zr_{0.125})$ precipitates isothermally aged at 425 °C after cold working and aging at 600 °C are shown in Figure 13. Typical microstructures after 20 and 400 hours of aging are shown in Figure 14. Since the tetragonal (DO_{23}) Al_3Zr platelets have been observed[9,21] to have {100} habit planes, TEM foils were tilted, whenever possible, to obtain a ⟨001⟩ zone axis. For the tetragonal plates, one-half of the particle's width cubed, r^3, is plotted *vs* time. The larger extrapolated initial particles size for the $Al_3(V_{0.875}Zr_{0.125})$ phase is the result of the double preaging treatment em-

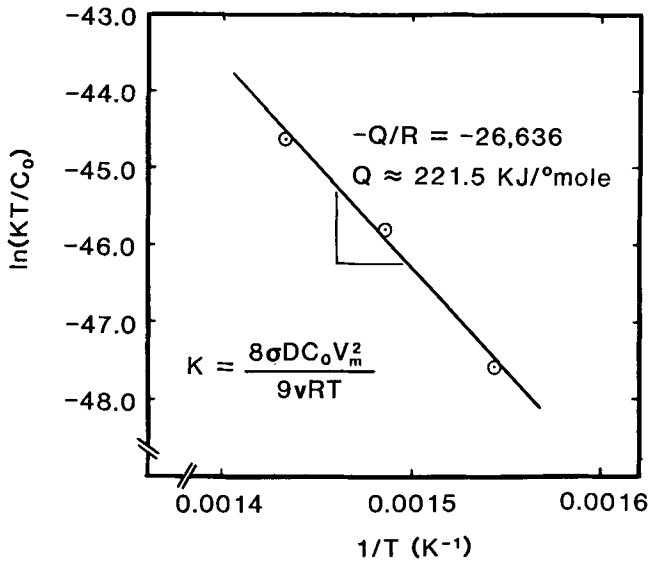

Fig. 12 — Determination of the activation energy, Q, for the coarsening of cubic $L1_2$ Al_3Zr precipitates from a plot of $\ln(KT/C_0)$ *vs* $1/T$.

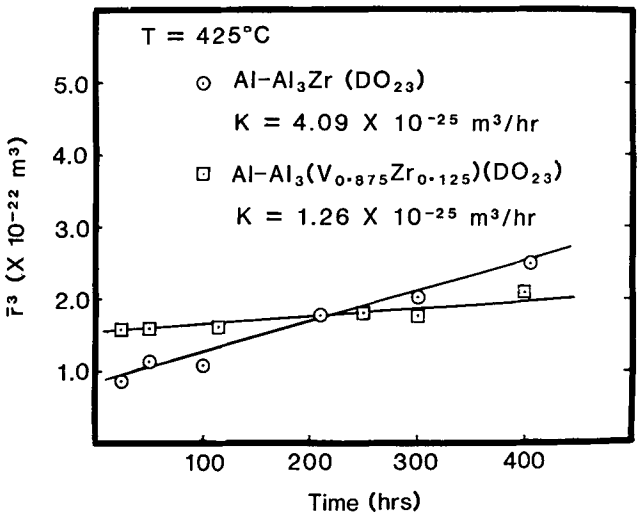

Fig. 13—Comparison of volumetric coarsening rate of tetragonal DO_{23} $Al_3(V_{0.875}Zr_{0.125})$ with Al_3Zr during isothermal aging at 425 °C. The particle size $\bar{r}$ is defined as half the average thickness of the plate-like particles across the minor axis of the image in the micrographs. The Al-Zr alloy was cold rolled 90 pct and preaged 50 h at 600 °C. The Al-V-Zr alloy was cold rolled an additional 5 pct and annealed an additional 50 h at 600 °C to convert it to the DO_{23} phase. Thus the short times particle size is much larger.

ployed to obtain a homogeneous dispersion of tetragonal precipitates.

The tetragonal (DO_{23}) $Al_3(V_{0.875}Zr_{0.125})$ particles coarsen in volume one-third slower at 425 °C than the (DO_{23}) Al_3Zr particles. This is most likely due to a reduction in overall mismatch (Eq. [3]) from 2.8 to 2.4 pct with a resulting reduction in the average interfacial energy of the particles. At 425 °C, the tetragonal (DO_{23}) Al_3Zr phase coarsens in volume 16 times faster than cubic ($L1_2$) Al_3Zr phase while tetragonal $Al_3(V_{0.875}Zr_{0.125})$ phase coarsens 8 times faster than cubic $Al_3(V_{0.875}Zr_{0.125})$ phase. These differences between the cubic ($L1_2$) and tetragonal (DO_{23}) particle coarsening rates are most certainly related to the higher average interfacial energies for the tetragonal particles.

Normalized experimental histograms of particle widths for each of the tetragonal phases at 20 and 200 hours are shown in Figures 15(a) through (d). For comparison, the steady state particle size distribution, $\rho^2 h(\rho)$, predicted by the LSW theory of VDC coarsening may be seen in Figures 9, 10, and 11. As may be observed, an opposite skewness and particle sizes much larger than the predicted maximum size were found. Similar disparities in the experimental histograms determined for other metallic

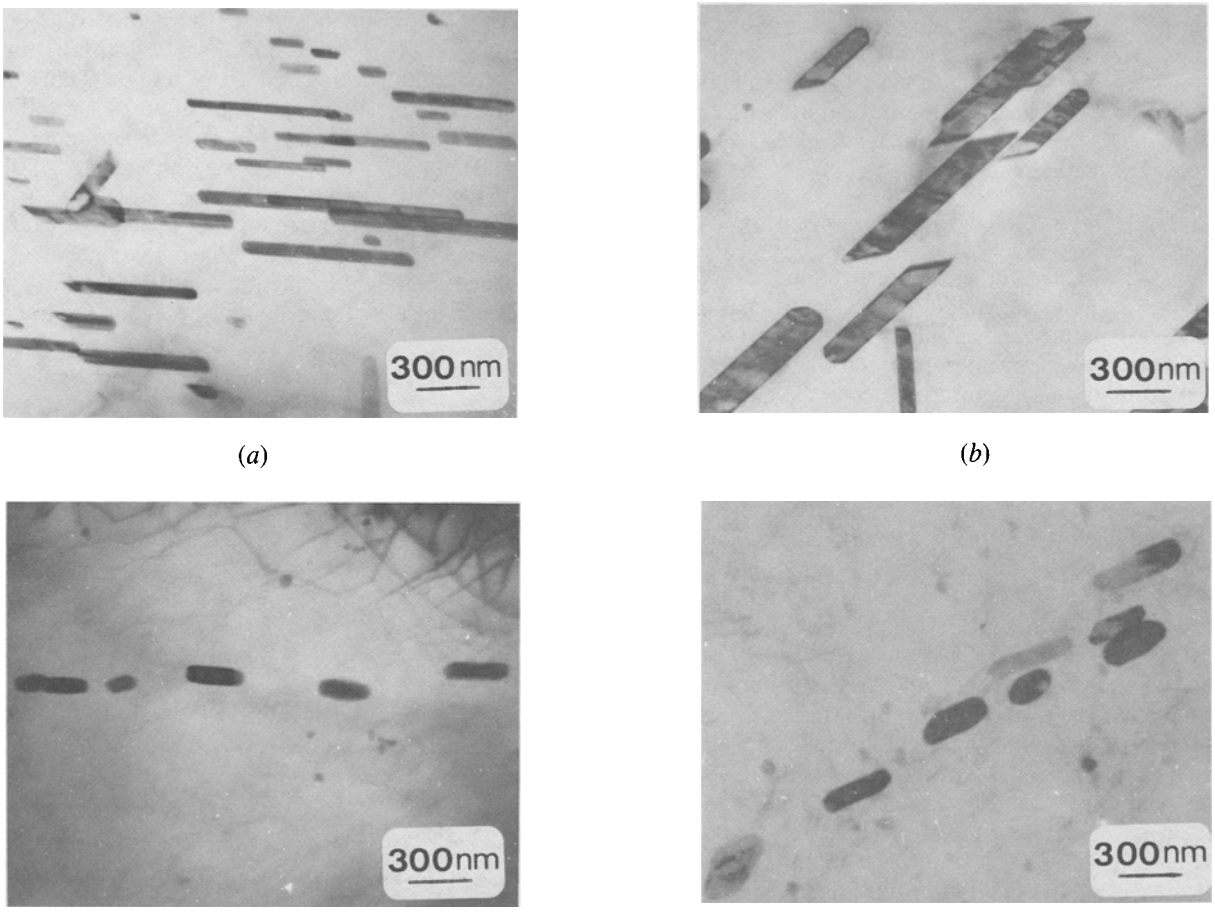

Fig. 14—TEM micrographs showing tetragonal DO_{23} Al_3Zr (*a*, *b*) and $Al_3(V_{0.875}Zr_{0.125})$ (*c*, *d*) precipitates after aging 20 (a, c) and 400 (b, d) h at 425 °C. Pretreatments are described in caption to Fig. 13.

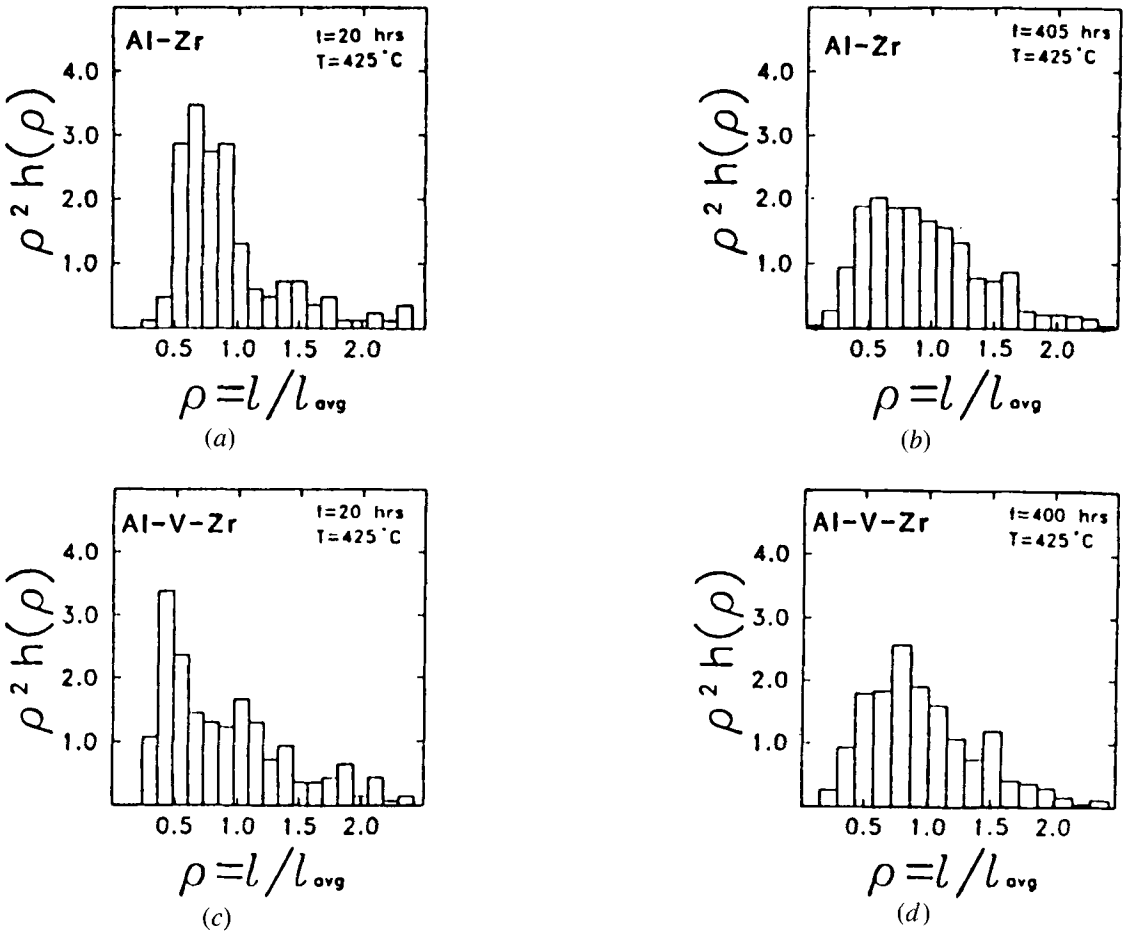

Fig. 15—Particle size distributions for tetragonal Al_3Zr (*a*, *b*) and $Al_3(V_{0.875}Zr_{0.125})$ (*c*, *d*) aged at 425 °C for 20 (a, c) and 400 h (b, d). Particle size is defined in the caption for Fig. 13.

systems containing nonspherical precipitates have been observed.[35–38] Presently, no theoretical treatments are available which adequately treat diffusion controlled coarsening of nonspherical particles. In addition, an interface mechanism control of coarsening must be considered for the DO_{23} platelets. Thus, based on the present results, we are not able to determine the rate controlling mechanism for Ostwald ripening of the tetragonal (DO_{23}) phase particles. While straight lines for an r^3 *vs* t relationship may be drawn through the data, essentially similar agreement may be obtained between r^2 and t. Thus, Figure 13 may not be taken as proof for the LSW theory of volume diffusion controlled coarsening (VDC) for this case.

There were no major changes in the average aspect ratios of the particles, *i.e.*, average width to length ratio. For the tetragonal Al_3Zr phase, this varied from 5.1 for 50 hours of aging to 4.7 for 405 hours of aging. Similarly, the average aspect ratio of the tetragonal $Al_3(V_{0.875}Zr_{0.125})$ particles varied from 2.9 for 50 hours of aging to 2.4 for 400 hours of aging. Since the particles are thickening and lengthening at about the same rate, the ledge growth mechanism proposed for the shape coarsening of θ' particles in Al-Cu alloys proposed by Merle and Fouquet[36,37] does not occur in the present system.

IV. FINAL DISCUSSION

Whether or not volume diffusion controls the rate of Ostwald ripening, reduction in the interfacial energy between the particles and matrix should reduce the ripening rate. This was borne out by the experimental results. Substituting vanadium for most of the zirconium reduced the mismatch between the cubic ($L1_2$) Al_3X phase and the matrix as well as the mismatch between the tetragonal (DO_{23}) Al_3X phase and the matrix. In both cases slower Ostwald ripening resulted. Further, the transformation of the $L1_2$ to the DO_{23} phase was much more sluggish in the Al-V-Zr alloy. The free energy change for the reaction $\alpha_{C_0'} + L1_2 \rightarrow \alpha_{C_0} + DO_{23}$ was reduced due to reduction in strain and interfacial energy. This is a very important principle which has consequences in other systems.

For Ostwald ripening of cubic Al_3Zr and $Al_3(V_{0.875}Zr_{0.125})$, VDC coarsening is proposed to be the rate controlling process even though calculation of the interfacial energy from the LSW theory is much too high. The origin of the discrepancy is not known to the authors. Enhanced diffusion due to imperfections may be playing a role.

Finally, does better lattice matching between the dispersed phase and matrix possibly lead to a better high temperature

alloy? Of course, extensive dispersed phase coarsening at the temperature of application possibly accelerated by creep or fatigue deformation would lead to overaging and reduction in strength and also possibly ductility. Thus a reduced particle coarsening rate is desirable. It is of interest to compare the present Al-Zr and Al-Zr-V alloys to a binary Al-Fe alloy. Presently, the Al-Fe system is the basis for development of a new series of high temperature Al alloys. The equilibrium dispersed phase in these systems at 425 °C is Al_3Fe which is incoherent with the matrix. In an Al-8 wt pct Fe alloy* the coarsening rate at 425 °C, corrected to 1 pct volume fraction of dispersed phase,[4] is 50 times faster than even tetragonal $DO_{23}Al_3Zr$. Thus the cubic ($L1_2$) and tetragonal (DO_{23}) Al_3X phase suitably alloyed to give good matching with the lattice parameter of the matrix are very promising as the basis for improved high temperature Al base alloys.

*This alloy, furnished by Alcoa Technical Center, was prepared by forging rapidly solidified powders. The coarsening rates were determined at Northwestern by Dr. Jain-Long Horng and Dr. Lynette Angers.

ACKNOWLEDGMENTS

The authors are pleased to acknowledge the support of the Air Force Office of Scientific Research, USAF, under Grant No. AFOSR 82-0005B. The use of the Central Facilities of Northwestern University's Materials Research Center sponsored under the NSF-MRL program (Grant No. DMR82-16972) is greatly appreciated. Professors M. Meshii and J. B. Cohen gave much assistance with the electron microscopy and X-ray diffraction, respectively. The authors acknowledge very helpful discussions with Professor Julia R. Weertman, Dr. Lynette Angers, Dr. Hector Calderon, and Mr. In Bae Kwon in our research group. Dr. Colin Adam, Allied Chemical Corporation, gave helpful advice.

REFERENCES

1. I. M. Lifshitz and V. V. Slyozov: *J. Phys. Chem. Solids*, 1961, vol. 19, p. 35.
2. C. Wagner: *Z. Elektrochem.*, 1961, vol. 65, p. 581.
3. P. W. Voorhees and M. E. Glicksman: *Metall. Trans. A*, 1984, vol. 15A, p. 1081.
4. A. D. Brailsford and P. Wynblatt: *Acta Metall.*, 1979, vol. 27, p. 489.
5. M. E. Fine: *Metall. Trans. A*, 1975, vol. 6A, p. 625.
6. G. Brauer: *Z. anorg. ally. Chem.*, 1939, vol. 242, p. 1.
7. F. J. J. van Loo and G. D. Rieck: *Acta Metall.*, 1973, vol. 21, p. 61.
8. C. M. Adam: in *Rapidly Solidified Amorphous and Crystalline Alloys*, B. H. Kear, B. C. Giessen, and M. Cohen, eds., Elsevier Science Pub. Co., Inc., 1982, pp. 411-22.
9. E. Nes: *Acta Metall.*, 1972, vol. 20, p. 499.
10. S. Tsunekawa and M. E. Fine: *Scr. Metall.*, 1982, vol. 16, p. 391.
11. M. Zedalis and M. E. Fine: *Scr. Metall.*, 1983, vol. 17, p. 1247.
12. D. J. McPherson and M. Hansen: *Trans. ASM*, 1954, vol. 46, p. 354.
13. A. Roth: *Z. Metallkunde*, 1940, vol. 32, p. 356.
14. P. Hirsch, A. Howie, R. B. Nicholson, D. W. Pashley, and M. J. Whalen: in *Electron Microscopy of Thin Crystals*, Robert E. Krieger Pub. Co., Inc., New York, NY, 1977, pp. 124-28.
15. J. W. Edington: in *Practical Electron Microscopy in Materials Science*, Von Nostrand Reinhold Co., New York, NY, 1976, pp. 83-84.
16. D. J. H. Cockayne, I. L. F. Ray, and M. J. Whelan: *Phil. Mag.*, 1969, vol. 20, p. 1265.
17. A. J. Ardell and R. B. Nicholson: *J. Phys. Chem. Solids*, 1966, vol. 27, p. 1793.
18. L. A. Willey: Alcoa Research Labs, 1957, cited in *Aluminum*, 1967, vol. I.
19. N. F. M. Henry and K. Lonsdale: in *International Tables for X-ray Crystallography*, 1952, vol. 1, pp. 79-90.
20. E. Nes and N. Ryum: *Scr. Metall.*, 1971, vol. 5, p. 987.
21. N. Ryum: *Acta Metall.*, 1969, vol. 17, p. 269.
22. O. Izumi and D. Oelschlagel: *Scr. Metall.*, 1969, vol. 3, p. 619.
23. M. Sundberg, R. Sundberg, and B. Jacobson: *Jernkontoret Ann.*, 1971, vol. 155, p. 1.
24. E. Nes and H. Billdal: *Acta Metall.*, 1977, vol. 25, p. 1031.
25. R. M. Fisher and M. J. Marcinkowski: *Phil. Mag.*, 1960, Ser. 8, vol. 8, p. 1385.
26. N. Ryum: *J. Mat. Sci.*, 1975, vol. 10, p. 2075.
27. P. A. Flinn: *Trans. TMS-AIME*, 1960, vol. 218, p. 145.
28. T. Marumo, S. Fujikawa, and Ken-ichi Hirano: *J. Japan Inst. Light Metals*, 1973, vol. 23, No. 1, p. 17.
29. H. Jones: in *Rapid Solidification Processing—Principles and Technologies II*, R. Mehrabian, B. H. Kear, and M. Cohen, eds., Claitor's Pub. Div., Baton Rouge, LA, 1980, pp. 306-16.
30. S. Hori, S. Saji, and T. Kobayashi: in *Technol. Report*, Osaka University, 1978, vol. 28, p. 359.
31. A. J. Ardell: *Acta Metall.*, 1968, vol. 16, p. 511.
32. P. K. Rastaogi and A. J. Ardell: *Acta Metall.*, 1971, vol. 19, p. 321.
33. H. Calderon and M. E. Fine: *Mat. Sci. Eng.*, 1984, vol. 63, p. 197.
34. H. A. Calderon, J. R. Weertman, and M. E. Fine: *Scr. Metall.*, 1984, vol. 18, p. 587.
35. J. D. Boyd and R. B. Nicholson: *Acta Metall.*, 1971, vol. 19, p. 1379.
36. P. Merle and F. Fouquet: *Acta Metall.*, 1981, vol. 29, p. 1919.
37. P. Merle and F. Fouquet: *Acta Metall.*, 1981, vol. 29, p. 1929.
38. D. Janoff and M. E. Fine: *Mat. Sci. Eng.*, 1984, vol. 64, p. 67.